R 31

TECHNION RESEARCH AND DEVELOPMENT FOUNDATION LTD.

TECHNION CITY, HAIFA 32000, ISRAEL

Annual Report on Research No. 160-573:

Multi-Disciplinary Optimization of Aeroservoelastic Systems

Sponsored by NASA Grant NAGW-1708

Principal Investigator: Dr. Mordechay Karpel

Faculty of Aerospace Engineering

M. Karpel

Principal Investigator

September 12, 1990

Date

© 1990 by Mordechay Karpel, National Aeronautics and Space Administration, and the Technion Research and Development Foundation Ltd.

(NASA-CR-187931) MULTI-DISCIPLINARY OPTIMIZATION OF AEROSERVOELASTIC SYSTEMS Annual Report, 1 Oct. 1989 - 30 Sep. 1990 (Technion Research and Development

N90-29585

Unclas

provided by NASA Technical Reports Server

brought to you by CORE

View metadata, citation and similar papers at core.ac.uk

The purpose of the research project "Multi-Disciplinary Optimization of Aeroservoelastic Systems" was to advance the methodology of multi-disciplinary optimization and to develop efficient analytical and computational tools for simultaneous structural and control system optimal design with aeroservoelastic constraints. These tasks have been accomplished successfully. The new analytical methods, computation codes and case studies developed during the course of this work extend the knowledge of this complex subject and supply the aircraft developer with practical guidelines and efficient computational tools for achieving integrated design goals in an optimal way.

The first part of the work, in which the Minimum-State aeroservoelastic modeling method has been extended to deal with large problems with varying parameters, has been reported in the interim report of March 1st, 1990. The main results of this part are summarized in Appendix A, which has been accepted for publication in the AIAA Journal, and utilized in the MIST computer code.

The second part of the research project included further developments of analytical and computational tools and a synthesis of an end-to-end optimization procedure from data-base construction to the numerical optimal design process. This part is summarized in Appendix B, which will be presented at the 3rd Airforce/NASA symposium on multi-disciplinary analysis and optimization in September 24-26, 1990, San Francisco, CA, and utilized in the FASER computer code.

Appendix A

Log No. J19006

Extensions to the Minimum-State Aeroelastic Modeling Method

Mordechay Karpel*
Technion - Israel Institute of Technology
Haifa, Israel 32000

Introduction

In order to account for unsteady aerodynamics in first-order, time-invariant state-space formulation of aeroelastic equations of motion, the aerodynamic forces have to be described as a rational function in the Laplace domain. The Minimum-State (MS) aerodynamic approximation method[1,2] was designed to minimize the number of aerodynamic states in the resulting aeroelastic model. References 2 and 3 applied the MS method to subsonic aeroservoelastic problems with one flutter mechanism and demonstrated a reduction of about 75% of the number of aerodynamic states relative to other methods with the same level of accuracy. The effectiveness of the MS method was increased by the introduction of a physical weighting technique[2] which weights each aerodynamic input data term according to its relative importance. Reference 4 used the MS formulation for additional reduction of the model size by dynamic residualization of high frequency structural states. The MS and the physical weighting procedures are extended in this paper to expand their efficiency and generality and to improve the dynamic residualization. Even though the formulation and numerical examples deal with structural-mode-related aerodynamics only, the extensions are applicable to control surface and gust related aerodynamics as well.

The MS Approximation Procedure

The MS method approximates the Laplace domain generalized aerodynamic force coefficient matrix by:

$$[\tilde{Q}_s(p)] = [A_0] + [A_1]p + [A_2]p^2 + [D](p[I] - [R])^{-1}[E]p \qquad (1)$$

*Senior Research Fellow, Faculty of Aerospace Engineering, Member AIAA

where p is the nondimensionalized Laplace variable p=sb/V, where b is a reference length and V is the true airspeed. The resulting time-domain state-space aeroelastic equations of motion are presented in Ref. 2. The number of aerodynamic states (m) is equal to the order to [R].

The input data are unsteady aerodynamic complex matrices $[Q_s(ik_l)]=[F(k_l)]+i[G(k_l)]$, calculated at several $p=ik_l$ points where each $k_l=\omega_l b/V$ is a tabulated reduced frequency. The approximation problem is to find the combination of the real valued $[A_0]$, $[A_1]$, $[A_2]$, [R], [D] and [E] of Eq. (1) that best fit the tabulated data. The mxm aerodynamic lag matrix [R] is diagonal with distinct negative values to be chosen by the analyst. The applications of Refs. 2 and 4 indicated that the results are not very sensitive to the lag values when they are spread over the range of tabulated k_l values. Three approximation constraints are applied to each term of $[Q_s]$ in order to reduce the problem size by explicitly determining $[A_0]$, $[A_1]$ and $[A_2]$. The formulation of Ref. 2 is extended here to allow more flexibility in constraint selection without increasing the problem size. The three constraints are: a) data match at $k_l=0$, which yields:

$$A_{0_{ij}} = F_{ij}(0) \tag{2}$$

b) real-part data-match at a non-zero $k_l=k_f$, or a zero coefficient constraint, which yield:

$$A_{2_{ij}} = \left[F_{ij}(0) - F_{ij}(k_f)\right]/k_f^2 + \{D_i\}^T\left[k_f^2[I]+[R]^2\right]^{-1}\{E_j\} \text{ or } A_{2_{ij}} = 0 \tag{3}$$

where $\{D_i\}^T$ is the ith row of [D] and $\{E_j\}$ is the jth column of [E]; and c) imaginary-part data-match at a non-zero $k_l=k_g$, or a zero coefficient constraint which yield:

$$A_{1_{ij}}=G_{ij}(k_g)/k_g+\{D_i\}^T\left[k_g^2[I]+[R]^2\right]^{-1}[R]\{E_j\} \quad \text{or} \quad A_{1_{ij}} = 0 \tag{4}$$

The approximation formula (1) and the constraint Eqs. (2), (3) and (4) yield an over determined set of approximate equations which are solved for [D] and [E] by an iterative, weighted least-square procedure which starts with an initial guess of [D]. The equations and the solution procedure are those of Ref. 2, modified to allow k_f of Eq. (3) and k_g of Eq. (4) to have different values for different aerodynamic terms, and to allow the data

match constraints to be replaced by zero coefficient constraints.

Approximation Constraints for Subsequent Dynamic Residualization

The MS aeroelastic model is used in Ref. 4 for a further reduction of the model size via dynamic residualization which eliminates the states associated with a subset of high frequency vibration modes, but retains most of their effects on the retained states. The coefficient matrices of Eq. (1) are partitioned into the retained (r) and eliminated (e) partitions:

$$; [A_i] = \begin{bmatrix} A_{i_{rr}} & A_{i_{re}} \\ A_{i_{er}} & A_{i_{ee}} \end{bmatrix} \text{ for } i = 0,1,2 \; ; [D] = \begin{bmatrix} D_r \\ D_e \end{bmatrix} \; ; [E] = [E_r \; E_e] \qquad (5)$$

Unlike the static residualization, which neglects all the e related partitions except for the A_0 terms, the dynamic residualization neglects only the $A_{1_{ee}}$, $A_{2_{ee}}$, $A_{2_{er}}$ and $A_{2_{re}}$ terms. The retained effects of $A_{1_{er}}$, $A_{1_{re}}$, D_e and E_e improve the accuracy of the residualized model without increasing its size. The attempt made in Ref. 4 to improve the dynamic residualization even further by constraining the neglected terms to be zero in the preceding MS procedure (in lieu of data match constraints) did not yield better results. The reason was that with $A_{1_{ee}}=0$ the approximation errors are increased significantly. This had a negative effect on the quality of the entire approximated aerodynamics (including that of the retained modes) because the MS procedure minimized a single total error parameter. The modification suggested here is to apply the least-square solutions for $[E_r]$ and $[D_r]$ with the data associated with the retained modes only. The $[D_e]$ and $[E_e]$ matrices are solved with the entire data. As a result, the approximated $[\tilde{Q}_{s_{rr}}]$ is not affected by the inclusion of the eliminated modes in the approximation procedure.

Physical Weighting

A physical weighting method which weights each term of the tabulated aerodynamic data

according to a "measure of importance" is presented in Ref. 2. The measure-of-importance matrix associated with $[Q_s(ik_\ell)]$ is:

$$[\hat{W}]_\ell = \left| \left(-[M_s]k_\ell^2 + i[B_s]k_\ell + [K_s] + q_n[Q_s(ik_\ell)] \right)^{-1} \right|^T \qquad (6)$$

where $[M_s]$, $[B_s]$ and $[K_s]$ are the generalized mass, damping and stiffness matrices and q_n is a nominal dynamic pressure. As shown in Refs. 2 and 3, the variations of the measure-of-importance terms of Eq. (6) with k may have very sharp peaks. In addition, the peak values of many terms may be several orders-of-magnitude smaller than other peaks. The resulting extreme variations of weights may cause unrealistic approximation curves. To ensure good results at k values which fall between the tabulated ones, and to facilitate the application of the resulting aeroelastic model to a variety of flow conditions, structural modifications and control parameters, it may be desired to widen the weight peaks and to scale up the extremely low weights. The peak widening is performed in n_{wd} cycles where, in each cycle, $\hat{W}_{ij}(k_\ell)$ is changed to be $\max\{\hat{W}_{ij}(k_{\ell-1}), \hat{W}_{ij}(k_\ell), \hat{W}_{ij}(k_{\ell+1})\}$ of the previous cycle. The weights to be applied in the MS procedure are then calculated by:

$$W_{ij\ell} = \hat{W}_{ij\ell} \left[\max\left\{ \frac{1}{\max_{i,j}\{\tilde{W}_{ij}\}}, \frac{W_{cut}}{\tilde{W}_{ij}} \right\} \right] \qquad (7)$$

where $\tilde{W}_{ij} = \max_\ell \left\{ \left| Q_{s_{ij}}(ik_\ell) \right| \hat{W}_{ij\ell} \right\}$

and where W_{cut} is defined by the analyst. In this way, the maximum weighted absolute value of each aerodynamic term falls between W_{cut} and 1.

Numerical Examples

The numerical examples deal with the mathematical model of the Active Flexible Wing (AFW) wind-tunnel model (described in Ref. 4) with symmetric boundary conditions at Mach 0.9. The Doublet Lattice tabulated oscillatory aerodynamic matrices were generated at 12 k_ℓ values between 0.0 and 2.0 using the STABCAR[5] computer code which was also employed to

calculate the baseline p-plane roots using the p-k method with ten vibration modes. The resulting root-locus plots are shown in Fig. 1 which indicates two flutter mechanisms. The flutter dynamic pressure and frequency of the first mechanism (second branch) are q_f=1.447 psi and ω_f=58.94 rad/sec (k_{flut}=0.21). The flutter results of the second mechanism (seventh branch) are q_f=4.247 psi; ω_f=194.43 rad/sec (k_{flut}=0.69).

The physical weightings were performed with q=1.2 psi. Two types of physical weightings are compared below. The first type (symbolized by P-0) is with the original measures-of-importance of Eq. (6), namely with no peak widening (n_{wd}=0) and with no upscaling (W_{cut}=0 in Eq. (7)). The second type (symbolized by P-2) is with the two peak-widening cycles (n_{wd}=2) and with W_{cut}=0.01. The maximal weighted magnitudes of the P-0 aerodynamic data terms are given in Table 1. The most important modes are 2, 3, 6, 7 and 10 which have the highest diagonal values. The off-diagonal values associated with these modes are also higher than those of most other terms. It can be noticed that about 50% of the terms in Table 1 are smaller than 0.01. These terms are scaledup to 0.01 in the P-2 case. Comparison of Table 1 with the aeroelastic behaviour of Fig. 1 indicates that the weighting is reasonable over the entire q range of interest.

i=	1	2	3	4	5	6	7	8	9	10
j=1	0.098	0.126	0.086	0.012	0.000	0.018	0.007	0.001	0.006	0.005
2	0.137	1.000	0.707	0.038	0.007	0.129	0.104	0.008	0.079	0.045
3	0.085	0.722	0.622	0.052	0.003	0.091	0.039	0.003	0.029	0.015
4	0.010	0.059	0.044	0.022	0.001	0.006	0.003	0.000	0.002	0.000
5	0.001	0.003	0.004	0.002	0.043	0.002	0.001	0.000	0.001	0.001
6	0.027	0.132	0.115	0.013	0.002	0.377	0.026	0.003	0.012	0.060
7	0.013	0.079	0.053	0.006	0.001	0.042	0.274	0.004	0.028	0.066
8	0.001	0.008	0.005	0.000	0.000	0.003	0.003	0.018	0.002	0.001
9	0.011	0.070	0.041	0.006	0.001	0.023	0.031	0.003	0.135	0.090
10	0.007	0.046	0.021	0.007	0.001	0.087	0.087	0.000	0.098	0.291

Table 1: Maximal weighted magnitudes of the aerodynamic data terms.

The flutter characteristics of the resulting state-space models have been found by a linear root-locus analysis with variable q. The quality of the approximations is evaluated by comparing the state-space results with STABCAR result. An overall measure in each case

is the RMS value of the percentage errors in the four flutter parameters (q_{f_1},ω_{f_1},q_{f_2} and ω_{f_2}). Comparisons between RMS flutter errors in non-weighted (N) cases and physically weighted (P-0 and P-2) cases are shown in Fig. 2. It can be observed that the P-2 cases generally yield the best results and that they are more consistent than the P-0 cases. Calculations at Mach 1.15 (not shown) exhibit similar results.

The root locus of the P-2 case with 6 aerodynamic lags, diag[R]={-0.2,-0.45,-0.8,-1.2,-1.7,-2.0} is compared in Fig. 1 to that of the reference STABCAR solution. It can be observed that the agreement is good over the entire ranges of frequency, damping and dynamic pressure. This indicates that the physical weights calculated at q_n are adequate over the entire range.

All the MS cases above were constrained to match the data at k=0.0 and at the highest tabulated reduced frequency, namely k_f=k_g=2.0. Data match constraints at k_t values close to either one of the two k_{flut} values caused a slight improvement in the respective flutter mechanism, but a slight increase of the overall RMS error measure by about 1%. An error increase of about 2% was obtained when $[A_2]$=[0] replaced the k_f constraints. Much more significant errors resulted from the replacement of the k_g constraints by A_1=0 even when applied to the aerodynamic terms associated with the highest frequency mode only. These errors were reduced considerably with the application of the new procedure for subsequent dynamic residualization.

To demonstrate the application of the modified MS approximations in subsequent flutter analysis with dynamic residualization, the P-2 model with 6 aerodynamic states has been extended to include the first 20 vibration modes (instead of 10). The MS approximations were performed with the special residualization constraints assigned to the last 10 modes. The reference case is flutter analysis with all the 20 vibration modes. Reduced-size flutter analyses were performed by eliminating a subset of high-frequency modes by either mode truncation, static residualization or dynamic residualization. Variations of flutter dynamic pressure percentage errors vs. number of eliminated modes are shown in Fig. 3 for the second flutter mechanism. Similar trends, but with smaller

errors, were obtained for the first flutter mechanism. These results demonstrate that MS aerodynamic approximations facilitate additional high accuracy model size reduction via dynamic residualization.

References

1. Karpel, M.: "Design for Active Flutter Suppression and Gust Alleviation Using State-Space Aeroelastic Modeling," Journal of Aircraft, Vol. 19, No. 3, March 1982, pp. 221-227.
2. Karpel, M.: "Time-Domain Aeroservoelastic Modeling Using Weighted Unsteady Aerodynamic Forces," Journal of Guidance, Control & Dynamics, Vol 13, No. 1, January 1990, pp. 30-37.
3. Tiffany, S.H. and Karpel, M.: "Aeroservoelastic Modeling and Applications Using Minimum-State Approximations of the Unsteady Aerodynamics," AIAA Paper 89-1188-CP presented at the AIAA/ASME/ASCE/AHS/ASC 30th Structural Dynamics and Materials Conference, Mobile, Alabama, April 1989, pp. 265-274.
4. Karpel, M.: "Reduced-Order Aeroelastic Models via Dynamic Residualization," Journal of Aircraft, Vol. 27, No. 5, May 1990, pp. 449-455.
5. Adams, W.M., Jr., Tiffany, S.H., Newsom, J.R. and Peele, E.L.: "STABCAR - A Program for Finding Characteristic Roots of Systems Having Transcendental Stability Matrices", NASA T.P. 2165, June 1984.

Figures

Figure 1: Root locus of the 10 mode subsonic AFW case.

Figure 2: RMS flutter errors resulting from MS aerodynamic approximations.

Figure 3: Flutter dynamic pressure errors of the second flutter mechanism vs. # of eliminated high-frequency modes.

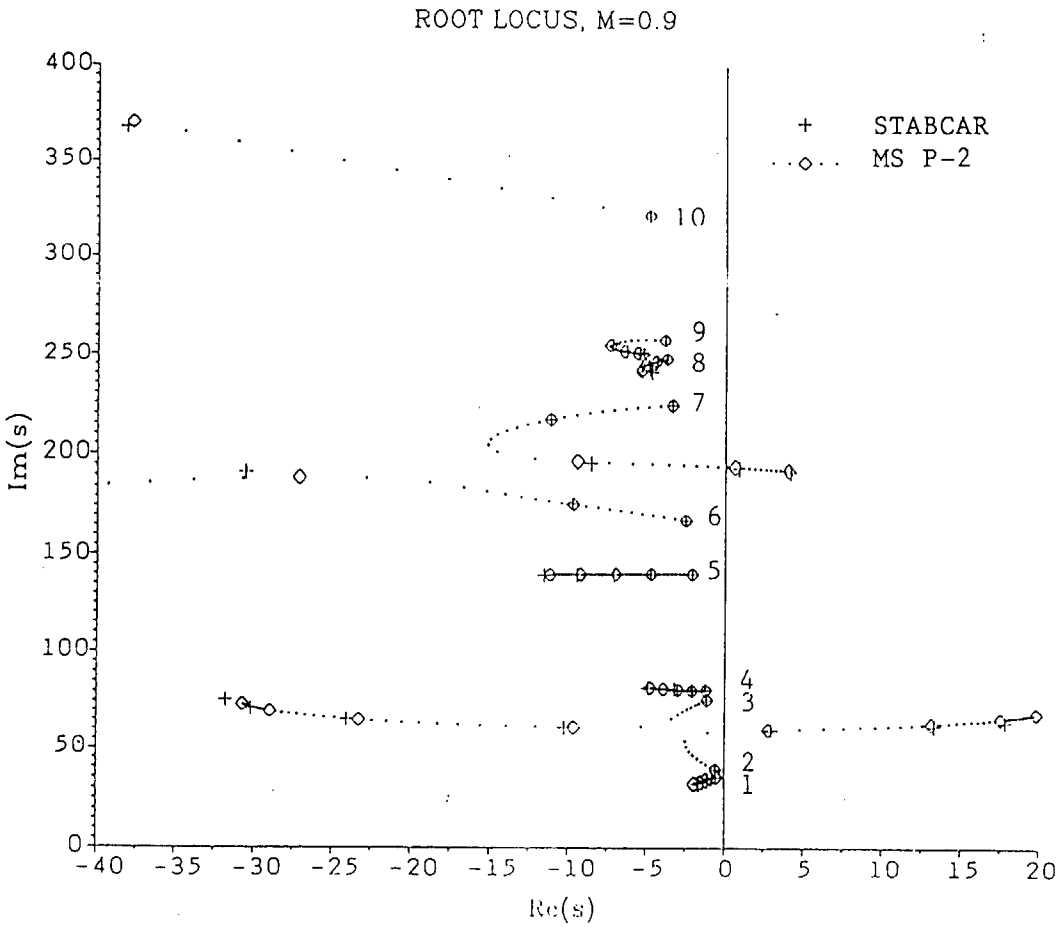

Figure 1 M. Kapel

ORIGINAL PAGE IS
OF POOR QUALITY

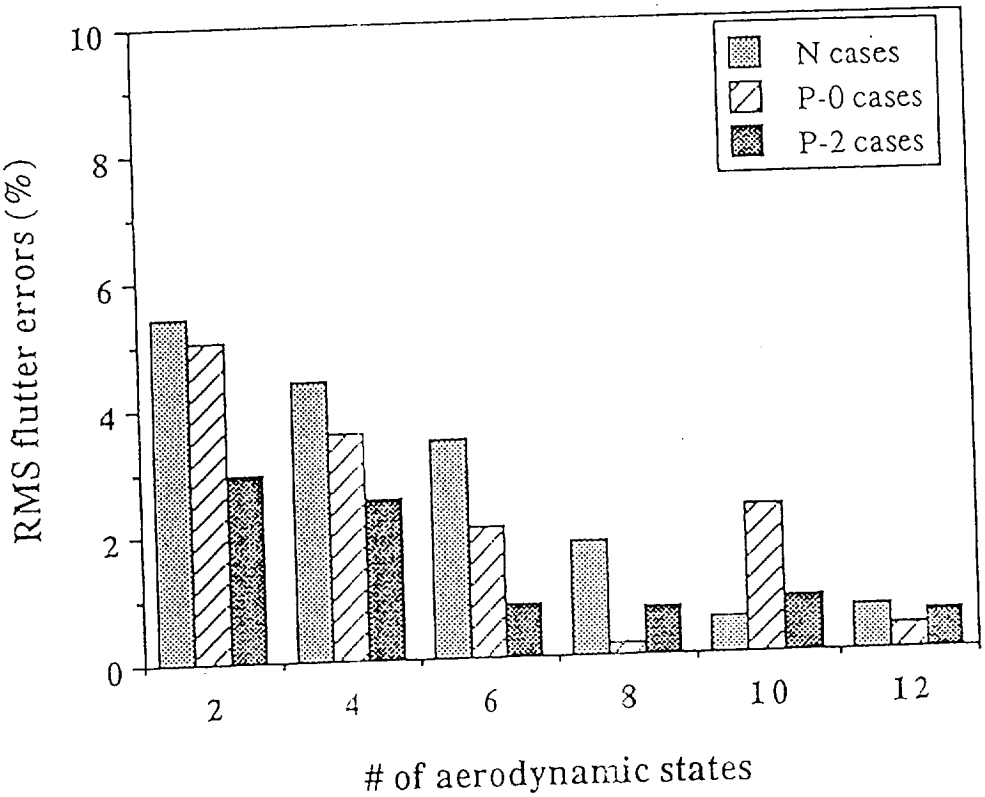
N cases
P-0 cases
P-2 cases
RMS flutter errors (%)
10
8
6
4
2
0
2
4
6
8
10
12
# of aerodynamic states

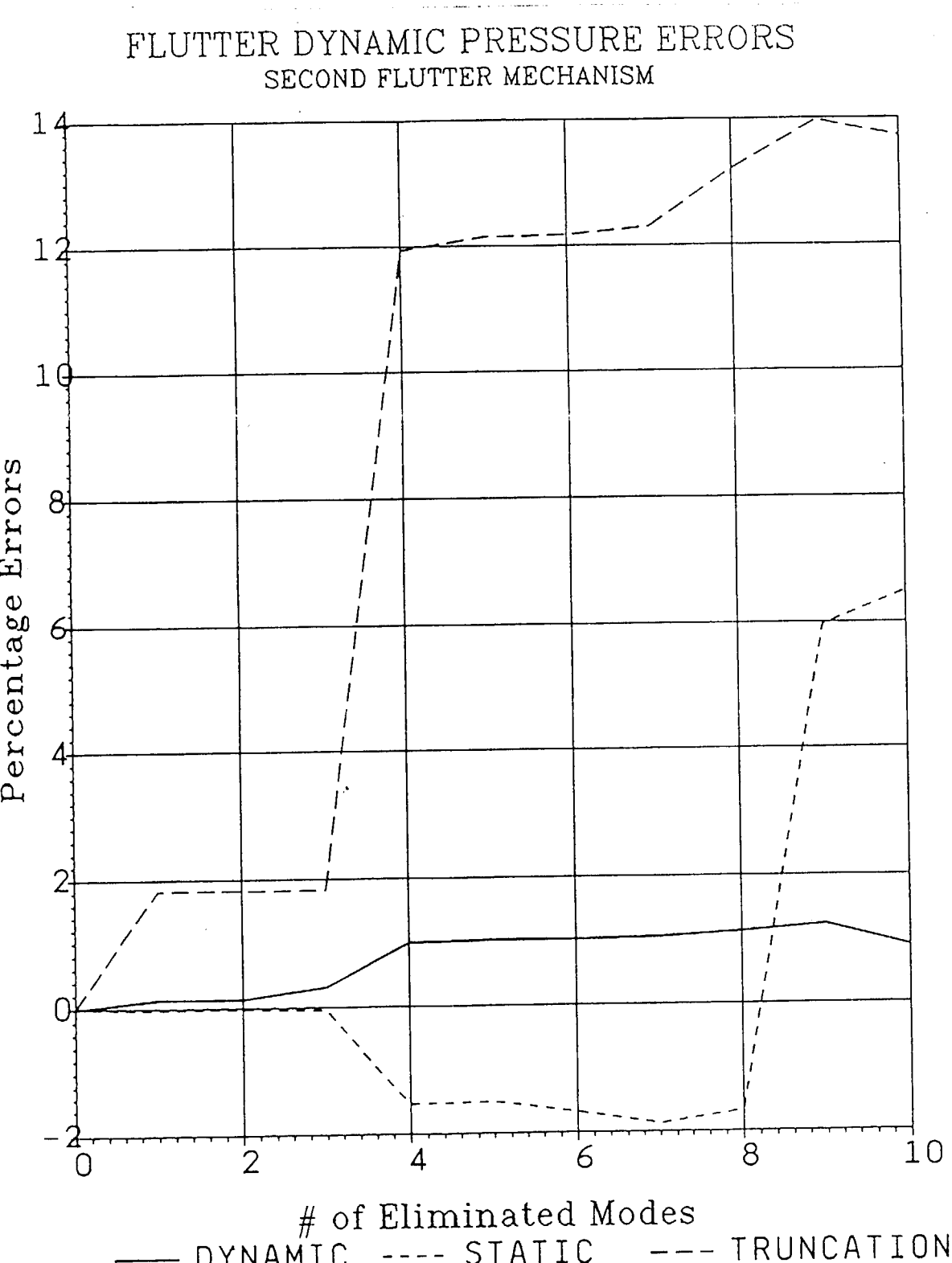

Figure 3

M. Kapel

Appendix B

Multidisciplinary Optimization of Aeroservoelastic Systems†

Mordechay Karpel*
Technion - Israel Institute of Technology
Haifa, Israel

Abstract

Efficient analytical and computational tools for simultaneous optimal design of the structural and control components of aeroservoelastic systems are presented. The optimization objective is to achieve aircraft performance requirements and sufficient flutter and control stability margins with a minimal weight penalty and without violating the design constraints. Analytical sensitivity derivatives facilitate an efficient optimization process which allows a relatively large number of design variables. Standard finite-element and unsteady aerodynamic routines are used to construct a modal data base. Minimum-state aerodynamic approximations and dynamic residualization methods are used to construct a high accuracy, low order aeroservoelastic model. Sensitivity derivatives of flutter dynamic pressure, control stability margins and control effectiveness with respect to structural and control design variables are presented. The performance requirements are utilized by equality constraints which affect the sensitivity derivatives. A gradient-based optimization algorithm is used to minimize an overall cost function. A realistic numerical example of a composite wing with four controls is used to demonstrate the modeling technique, the optimization process, and their accuracy and efficiency.

Introduction

The design of the structural and control systems of a flight vehicle with a given aerodynamic configuration starts with separate analyses which are aimed at satisfying basic stress and performance requirements. These preliminary designs are then optimized to satisfy structural and control stability margin requirements with a minimal performance cost and without violating the design constraints. Modern high-performance, control-augmented aircraft may have a strong coupling between the structural and control systems through aeroelastic effects. This calls for a multidisciplinary optimization process in which structural and control design variables are modified simultaneously.

The purpose of this work is to present a practical and efficient optimization scheme in which the various aeroservoelastic aspects are analyzed and synthesized with a common model. The applicability of this approach to realistic design cases has been demonstrated by Livne et al.[1] who presented an integrated synthesis scheme that can treat a rich variety of behaviour constraints and performance measures such as stress, displacements, control surface travel and hinge moments, aeroservoelastic poles, gust response, drag

---

†Supported by NASA Grant NAGW-1708
*Senior Research Fellow, Faculty of Aerospace Engineering

and aircraft maneuver parameters. A thorough literature survey is also given in Ref. 1. The structural model of Ref. 1 is based on the equivalent plate approach of Giles[2] with which a complex structure can be represented by a relatively low number of degrees of freedom. This allows the inclusion of the entire structural model in the aeroservoelastic model, which is impractical with common finite-element models like those of NASTRAN.

The optimization suggested in this paper can start with any structural and aerodynamic linear models, which has an advantage in practical applications. It is assumed that the structure can be represented in the optimization by a limited set of low-frequency vibration modes of the base-line model. The general scheme of a major optimization cycle is given in Fig. 1. An aeroelastic modal data base is first constructed for a relatively large number of modes.

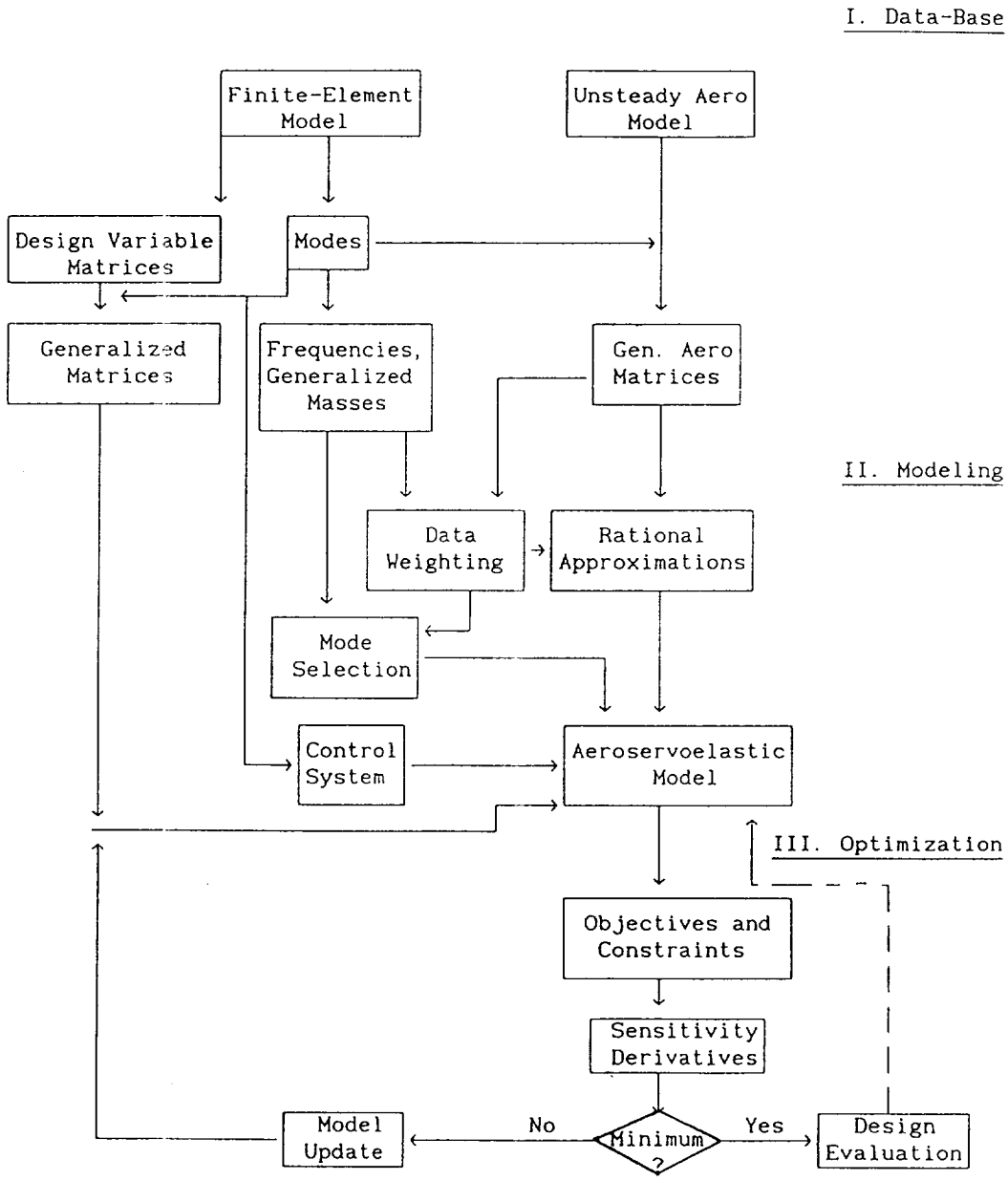

Fig. 1. The general scheme of a major optimization cycle.

The computational efficiency of this part is not as important as that of the later parts because it is performed once for the entire optimization process or at least for the major part of it. The aeroservoelastic modeling part of the scheme is aimed at resulting in a model of minimal size, but still accurate enough for the optimization process. Several size-reduction techniques are combined to achieve this goal and to provide the analyst with physical insight and numerical measures for an a priori evaluation of the size-reduction effects. The third part of the optimization scheme is the actual model update process to minimize a cost function within the design constraints. High computational efficiency of this part facilitates an interactive design process where the design can inspect the results and change parameters in order to perform trade-off studies and to obtain realizable design.

More details, analyticals development and numerical applications are given in the following sections. For the sake of clarity we start with the description of the test-case model that will be used to demonstrate the various parts of the optimization process. The formulation and applications are limited in scope to allow elaboration on the new features of this work.

The Test Case Model

The test-case deals with the Active-Flexible-Wing (AFW) composite wind-tunnel model tested at NASA Langley Research Center. A top view of the NASTRAN finite-element model is given in Fig. 2. A description of the aerodynamic model

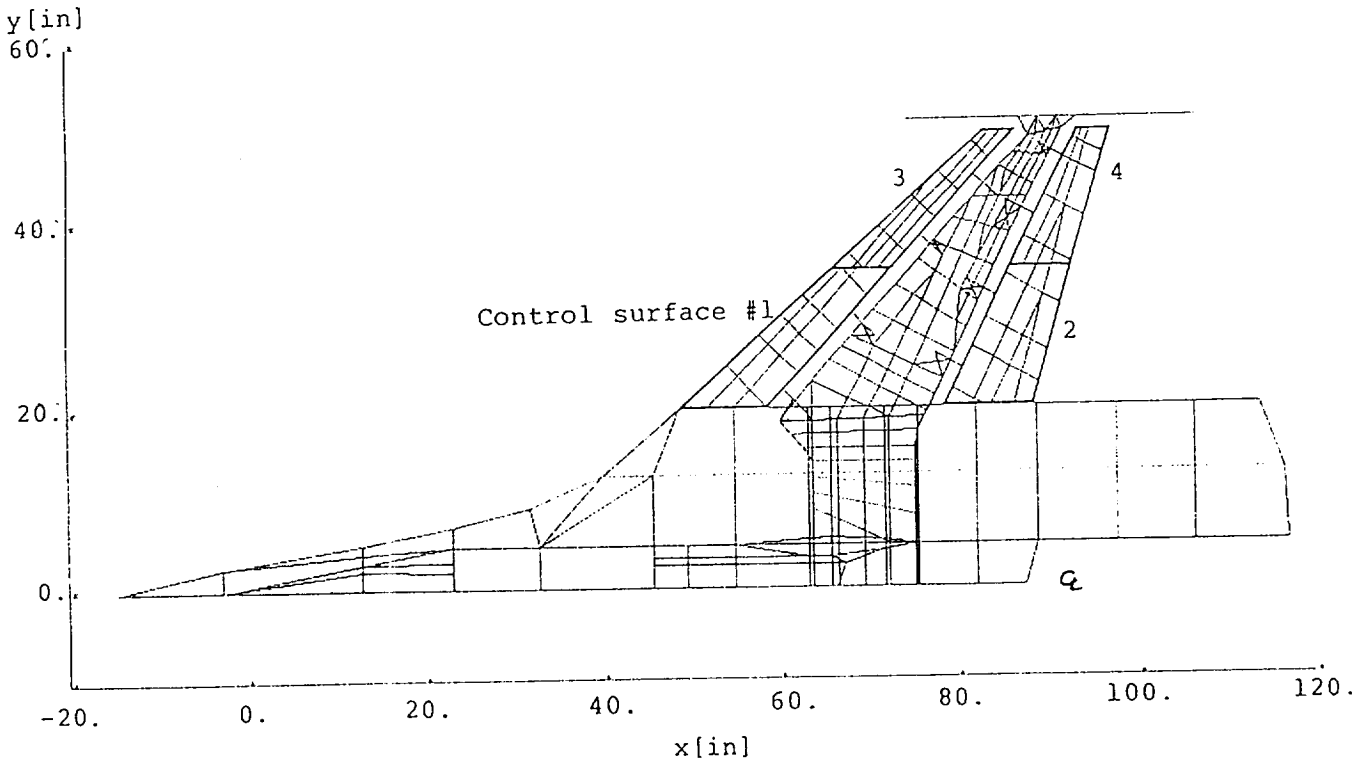

Fig. 2. Top view of the AFW structural model.

appears in Ref. 3. The mathematical model assumes antisymmetric boundary conditions at Mach 0.9. The lowest 12 vibration frequencies and the associated mode descriptions appear in Table 1.

Mode #	Frequency (Hz)	Description
1	0.	Rigid body roll
2	7.023	1st fuselage bending
3	7.856	1st wing bending
4	13.069	Missile pitch
5	16.161	2nd fuselage bending
6	27.408	2nd wing bending
7	38.271	1st wing torsion
8	39.639	Missile yaw
9	41.137	Fuselage torsion
10	49.922	3rd fuselage bending
11	51.640	3rd wing bending
12	57.403	2nd wing bending

Table 1: Natural Frequencies and Modes of the Base-Line Structure

The subject for optimization is the wing-box structure between y=18.45 in and y=49.30 in. The wing-box composite upper and lower skins are mirror images of each other. The wing-box is divided into 11 optimization zones as shown in Fig. 3. The base line weight of the optimized portion of the structure is 3.06 lb. The total number of high-strength graphite-epoxy plies in each of the skins varies between four at zone 2 (one in each of the 0°, $+45^\circ$, -45° and 90° orientations) and twenty at zone 9 (four in 0° and two in each of the 28°, -62°, 45°, -45°, 73°, -17° and 90° orientations).

The model has 4 control surfaces per wing (see Fig. 2) driven by third-order actuators. A zero-order control system reads the output of a roll rate-gyro located near the centerline and commands the actuators through different gains. A performance analysis established that a control law which supplies a rolling moment of L=-3000 lb-in per unit aircraft roll velocity (minus pilot roll command) is required for adequate roll performance at the design dynamic pressure q_d=1.5 psi. This yields the equality constraint

$$\Sigma G_i \eta_i \bar{L}_{\delta_i} = L/q_d \qquad (1)$$

where $\bar{L}_{\delta_i}$ is the rigid aerodynamic rolling moment per unit dynamic pressure due to unit deflection of the ith control surface and G_i and η_i are the associated control gain and aeroelastic effectiveness. In addition, the closed-loop

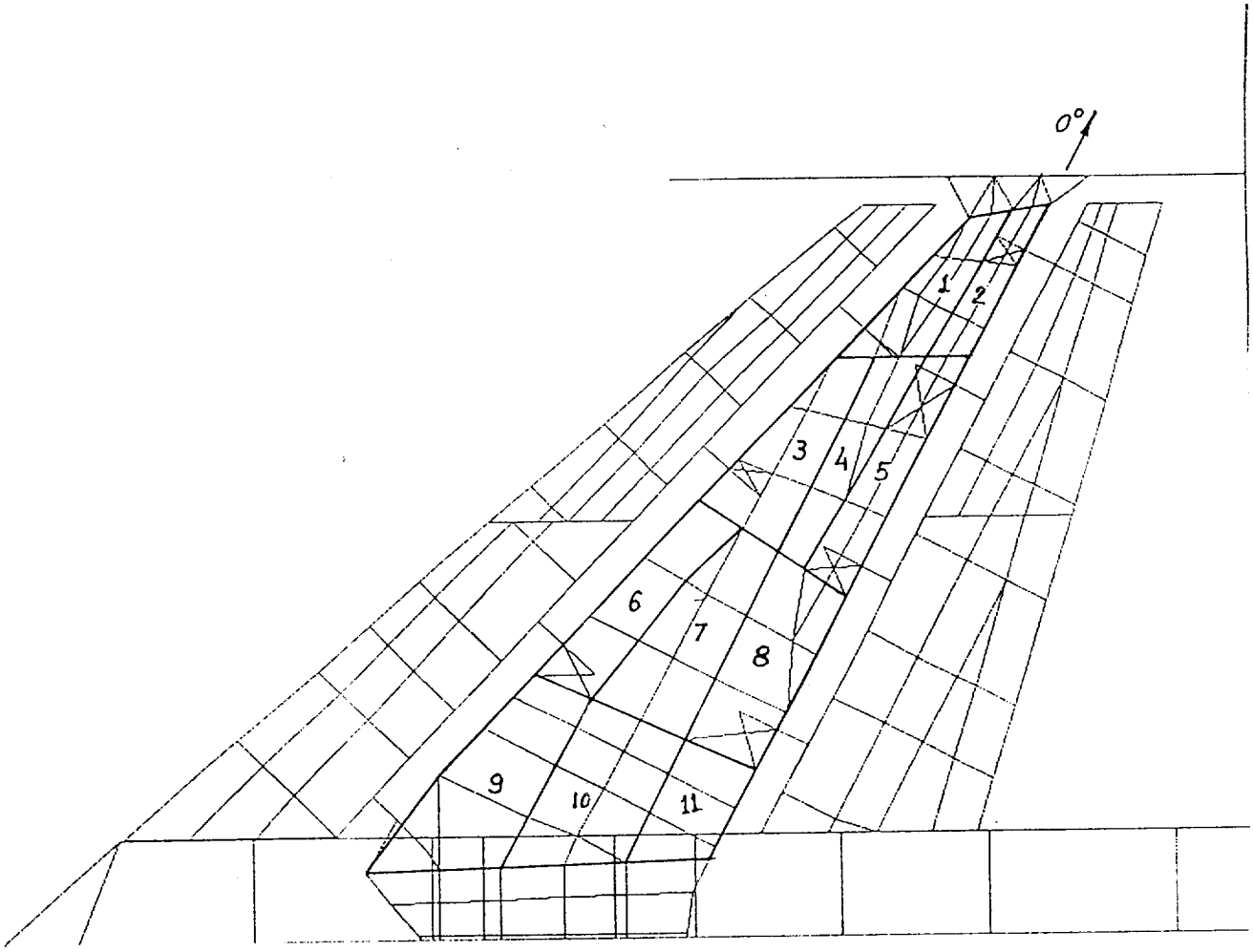

Fig. 3. Wing-box optimization zones.

aeroservoelastic system is required to exhibit a sufficient flutter margin

$$q_f \geq 1.44\, q_d \tag{2}$$

All the non-zero gains are required to exhibit sufficient gain margins

$$|GM_i| \geq 6 \text{ db} \tag{3}$$

where $GM_i = 20 \log(G_i^*/G_i)$ where G_i^*/G_i is a positive factor by which G_i has to be multiplied to achieve instability at q_d (with other gains remain unchanged). $G_i^*/G_i > 1$ yields the positive gain margin and $G_i^*/G_i < 1$ yields the negative one. Phase margin requirements and their sensitivity derivatives are given in Ref. 4. They are not discussed here because they are not critical in the test-case problem of this paper.

The Aeroelastic Data-Base

The aeroelastic data-base (see top part of Fig. 1) has been constructed using the NASTRAN code. The modes consist of the 25 lowest frequency vibration modes of the base-line structure, $[\psi_m]$, and 4 control surface deflection modes,

$[\psi_c]$, of unit rotation of the respective control surface and zero deflective elsewhere. The modes serve as generalized coordinates in the Laplace domain equation of motion

$$\left(\left[M_s\right]s^2 + \left[B_s\right]s + \left[K_s\right] + q\left[Q_s(s)\right]\right)\left\{\xi(s)\right\} = -\left(\left[M_c\right]s^2 + \left[Q_c(s)\right]\right)\left\{\delta(s)\right\} \quad (4)$$

where $[M_s]$, $[B_s]$ and $[K_s]$ are the generalized structural mass, damping and stiffness matrices respectively, $[M_c]$ is the control coupling mass matrix, $\{\xi\}$ is the vector of generalized structural displacements, $\{\delta\}$ is the vector of control surface commanded deflections, $[Q_s(s)]$ and $[Q_c(s)]$ are the generalized unsteady aerodynamic force coefficient matrices and q is the dynamic pressure. For the base-line structure $[M_s]$, $[K_s]$ and $[B_s]$ are diagonal where the first two were calculated from the finite element model and $[B_s]$ was constructed with structural damping of 0.01. $[M_c]$ can be calculated by

$$\left[M_c\right] = \left[\psi_m\right]^T\left[M\right]\left[\psi_c\right] \quad (5)$$

where [M] is the mass matrix in discrete coordinates. A convenient way to calculate $[\psi_c]$ and $[M_c]$ is by disconnecting the control surfaces from the actuators in the finite-element model and adding degrees-of-freedom representing $\{\delta\}$. These degree-of-freedom are mounted in the normal modes analysis by a fictitious mass matrix $[M_f]$ of large magnitudes. The test-case analysis was performed with the 4x4 $[M_f]$ matrix equal $[I]10^6$ while the maximum value of the other terms in the mass matrix is less than 1. The resulting modes include $[\psi_c]$ as rigid-body modes while the other modes, frequencies and generalized masses remain practically identical to those of the original structure. Each control surface mode is normalized to a unit deflection of the respective δ_i. Orthogonality implies

$$\begin{bmatrix} \psi_m \\ \psi_{mf} \end{bmatrix}^T \begin{bmatrix} M & 0 \\ 0 & M_f \end{bmatrix} \begin{bmatrix} \psi_c \\ I \end{bmatrix} = [0] \quad (6)$$

where the matrices are partitioned according to the original coordinates and the added ones. Equations (5) and (6) yield

$$\left[M_c\right] = -\left[\psi_{mf}\right]^T\left[M_f\right] \quad (7)$$

which is of course much more computationally efficient than Eq. (5).

The unsteady aerodynamic code is employed to calculate $[Q_s]$ and $[Q_c]$ of Eq. (4) (using $[\psi_m]$ and $[\psi_c]$) for various values of the nondimensionalized Laplace variable $\bar{s}=ik$ where k is the reduced frequency $\omega b/V$ where ω is the vibration

frequency, b is a reference semi-chord and V is the flow velocity. The aerodynamic data-base of the test-case include 13 generalized aerodynamic matrices for the k_ι values of 0., 0.05, 0.1, 0.2, 0.3, 0.4, 0.5, 0.7, 1.0, 1.4, 1.9, 2.5 and 3.1.

The remaining part of the aeroelastic data-base is the data needed for the structural optimization. The unit value of a structural design variable p_s in our case represents one composite fiber ply added to the upper and lower surfaces of one of the zones of Fig. 3. Three design variables, representing the 0°, 45° and -45° orientations are assigned for each zone. The stiffness and mass matrices, $[K_i]$ and $[M_i]$ associated with p_{s_i} are calculated by the finite-element code and pre and post multiplied by the appropriate partitions of $[\psi_m]$ to yield

$$\frac{\partial[K_s]}{\partial p_{s_i}} = [\psi_m]^T[K_i][\psi_m] \; ; \; \frac{\partial[M_s]}{\partial p_{s_i}} = [\psi_m]^T[M_i][\psi_m] \tag{8}$$

Expressions for the derivative of $[M_c]$ with respect to p_{s_i} are given in Ref. 4. In our case $\partial[M_c]/\partial p_{s_i}=0$ because the structure of the control surfaces is not modified throughout the optimization. The geometrical changes due to adding plies to the wing surface (stacking effects) are assumed to be negligible.

Aeroservoelastic Modeling

The aeroservoelastic modeling process (see part II of Fig. 1) is aimed at obtaining an efficient constant coefficient, state-space model to be used in the simultaneous structural and control optimization. To do so, the tabulated $[Q_s(ik_\iota)]$ and $[Q_c(ik_\iota)]$ matrices have to be approximated by rational functions. A review and extensions to the most common rational approximation methods and the associated model formulations are given in Ref. 5. Among those, the Minimum-State (MS) method[6,7] has been shown in several applications to realistic problems[7,8,9] to yield the most efficient aeroservoelastic models per desired accuracy. Best MS results are obtained when the physical weighting algorithm of Refs. 7 and 10, which weights the tabulated aerodynamic term according to their aeroservoelastic importance, is applied. The $[Q_s(ik_\iota)]$ terms are weighted according to their effect on the determinant of the system matrix on the left hand side of Eq. (4), calculated at the tabulated $s=ik_\iota b/V$ points, and the $[Q_c(ik_\iota)]$ terms are weighted according to their effect on the return signal in a Nyquist analysis performed with all the gains having the same non-zero values. The aerodynamic matrices associated with the 25 vibration modes and the 4 control modes were approximated with 6 MS approximation roots, which yield only 6 aerodynamic augmenting states.

The formulation of the resulting aeroservoelastic model is developed in Refs. 4 and 7. The closed-loop equation of motion for stability analysis reads

$$\{\dot{x}\} = [\bar{A}]\{x\} \tag{9}$$

where $[\bar{A}]$ is the closed-loop system matrix and $\{x\}$ is the state vector combined of the structural states $\{\xi\}$ and $\{\dot{\xi}\}$, the aerodynamic augmenting states $\{x_a\}$ and the control system states $\{x_c\}$. In our case, the full-size model has n=68 states (50 structural, 6 aerodynamic and 12 control states). The eigenvalues of the constant coefficient, real-valued matrix $[\bar{A}]$ are used to analyze the system stability. Root locus analysis with variable q yields the flutter dynamic pressure, q_f, at which one of the root branches crosses to the right hand side of the Laplace domain. The gain margins of Eq. (3) are found by a similar analysis with variable G_i which yields the instability gain G_i^*. More details and numerical examples for the calculation of flutter, gain and phase margins are given in Ref. 4. The accuracy of the MS approximation in the test-case has been examined by comparing flutter results with those of NASTRAN (using the PK method). The differences in q_f and ω_f were less than 1%.

Model Size-Reduction

The computational efficiency of the optimization process is approximately proportional to n^3. It is therefore desired to reduce n as much as accuracy allows. The vibration modes are divided for this purpose into three groups, those which may be truncated, those which may be eliminated via residualization, and those which remain in the model as independent states. The physical weighting algorithm described above and in Ref. 7 has been found to be a helpful guide in the mode selection-process. Two measures of aeroservoelastic importance are assigned to each mode. The measures are

$$Q_{1_i}^* = \max_{j,\iota}\left\{W_{ij\iota}\left|Q_{s_{ij}}(ik_\iota)\right|\right\} \tag{10}$$

and

$$Q_{2_i}^* = \max_{j,\iota}\left\{W_{ij\iota}\left|Q_{c_{ij}}(ik_\iota)\right|\right\}$$

where $W_{ij\iota}$ is the physical weight assigned to the (i,j) term of either the tabulated $[Q_s(ik_\iota)]$ or $[Q_c(ik_\iota)]$. The modal measures of aeroservoelastic importance of 17 of the 25 data-base modes are given in Table 2 in decreasing order of overall importance. The remaining 8 modes, for which both $Q_{1_i}^*$ and $Q_{2_i}^*$ are less than 0.01, are truncated in the optimization process. The 6 modes in the 2nd group of Table 2 are eliminated via residualization and the 11 modes in the first group of Table 2 are retained as independent variables.

Mode #†	Q_1^*	Q_2^*	Mode #	Q_1^*	Q_2^*
1	0.482	1.000	5	0.022	0.035
4	1.000	0.125	8	0.031	0.009
3	0.611	0.404	16	0.033	0.003
6	0.512	0.035	18	0.024	0.007
12	0.264	0.034	24	0.023	0.005
2	0.149	0.114	25	0.024	0.003
11	0.161	0.035	22	0.019	0.004
7	0.175	0.023	13	0.017	0.004
9	0.135	0.026			

†The other modes have Q* values of less than 0.01

Table 2: Modal Measures of Aeroservoelastic Importance

The truncation is performed by crossing out the associated rows on columns in $[\bar{A}]$ of Eq. (7). The truncated $[\bar{A}]$ satisfies

$$\begin{bmatrix} \bar{A}_{11} & \bar{A}_{12} \\ \bar{A}_{21} & \bar{A}_{22} \end{bmatrix} \begin{Bmatrix} U_1 \\ U_2 \end{Bmatrix} = i\omega_f \begin{Bmatrix} U_1 \\ U_2 \end{Bmatrix} \tag{11}$$

where subscripts 1 and 2 relate to the retained and residualized states respectively, and $\{U\}$ is the complex column eigenvector related to $s=i\omega_f$. The residualization in this work is performed by the dynamic method of Ref. 3. The residualized system matrix $[\tilde{A}]$ satisfies

$$\left[\tilde{A}\right]\left\{U_1\right\} = i\omega_f\left\{U_1\right\} \tag{12}$$

It is assumed that the differences between ω_f and $\{U_1\}$ of Eq. (11) and those of Eq. (12) are negligible. Consequently, the flutter eigenvalue and eigenvector of $[\tilde{A}]$ are used to calculate $\{U_2\}$ from the bottom partition of Eq. (11).

The effects of truncation and residualization on q_f and its derivative with respect to p_{s_2} are shown in Fig. 4. The solid lines give the percentage errors introduced by truncation vs. the number of truncated modes. The base-line values of q_f=1.736 psi and $\partial q_f/\partial p_{s_2}$=0.188 psi have been obtained with the full 25 mode model where the gain values associated with the four control surfaces are 0.0, -0.1, -0.1 and 0.0664 respectively. The modes truncated at each point of Fig. 4 are those with the lowest measures of aeroservoelastic importance

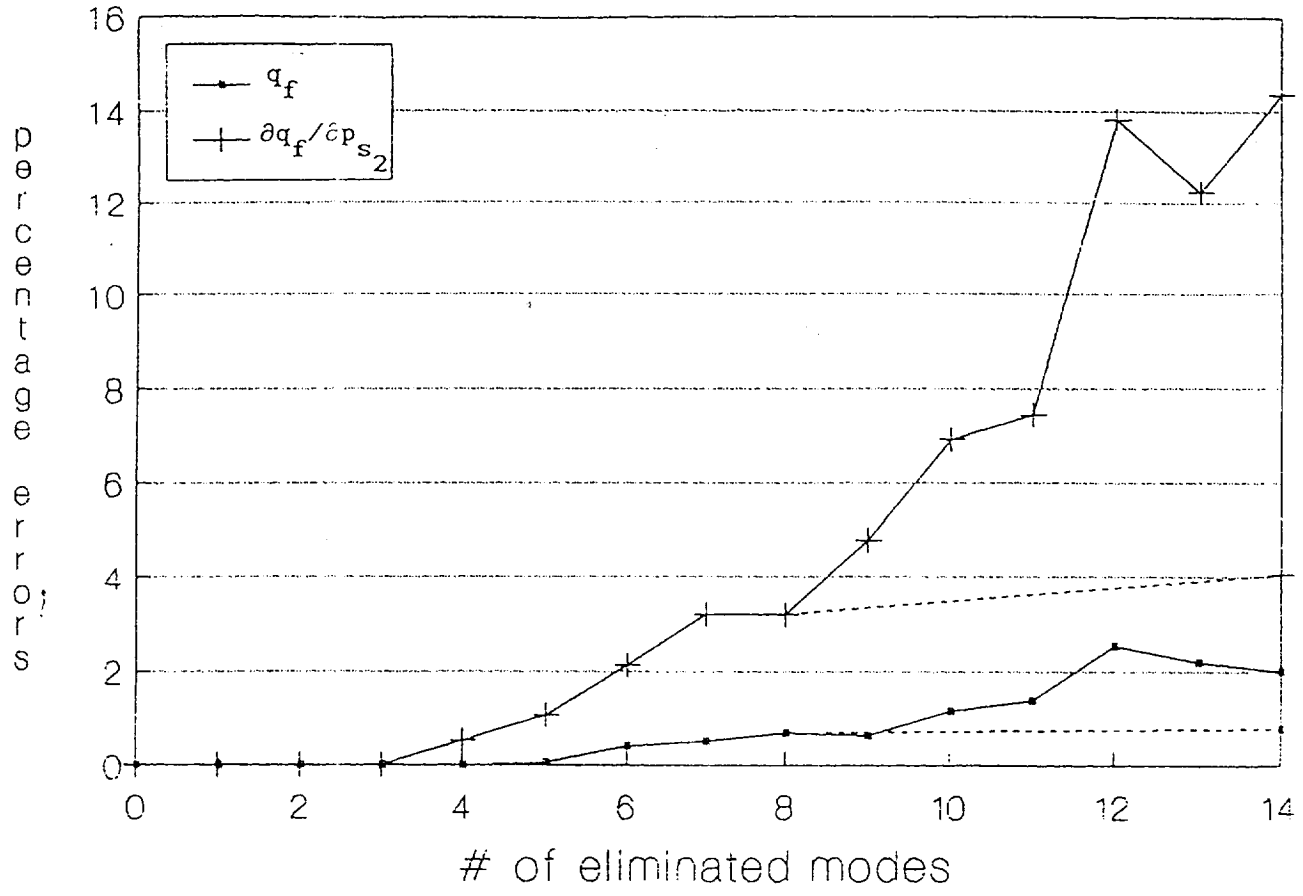

Fig. 4. Size-reduction effects on flutter dynamic pressure.

defined in Eq. (10). It can be deduced from the error rates of change that the usage of these measures for mode selection is adequate. The errors due to the truncation of 8 modes and residualization of 6 modes, also given in Fig. 4, demonstrate the accuracy of the dynamic residualization relative to that of truncation.

Control Effectiveness

The expressions for the aeroelastic control effectiveness parameters of Eq. (1) and their sensitivity derivatives follow the modal approach of Ref. 11. The real-valued $[Q_s(0)]$, $[Q_c(0)]$ and $[K_s]$ of Eq. (4) are partitioned into the rigid and elastic mode partitions:

$$\left[Q_s(0)\right] = \begin{bmatrix} \bar{Q}_{s_{11}} & \bar{Q}_{s_{12}} \\ \bar{Q}_{s_{21}} & \bar{Q}_{s_{22}} \end{bmatrix} ; \quad \left[Q_c(0)\right] = \begin{bmatrix} \bar{Q}_{c_1} \\ \bar{Q}_{c_2} \end{bmatrix}$$

and (13)

$$\left[K_s\right] = \begin{bmatrix} 0 & 0 \\ 0 & \bar{K}_s \end{bmatrix}$$

When there is a single rigid body mode in roll, the effectiveness of rolling moment due to unit deflection of the i-th control surface is

$$\eta_j = 1 - \frac{q_d}{\bar{Q}_{c_{1_j}}} \left[\bar{Q}_s\right]_{12} \left[B\right]^{-1} \left\{\bar{Q}_c\right\}_{2_j} \tag{14}$$

where $\{\bar{Q}_c\}_{2_j}$ is the j-th column of $[\bar{Q}_c]_2$ and

$$[B]=[\bar{K}_s]+[\Delta\bar{K}_s]+q_d[\bar{Q}_s]_{22} \; ; \; \left[\Delta\bar{K}_s\right] = \sum_i \frac{\partial[\bar{K}_s]}{\partial p_{s_i}} p_{s_i} \tag{15}$$

where $\partial[\bar{K}_s]/\partial p_{s_i}$ is calculated by Eq. (6) using elastic modes only. The differentiation of Eq. (14) with respect to a structural design variable p_{s_i} yields:

$$\frac{\partial \eta_i}{\partial p_{s_i}} = \frac{q_d}{\bar{Q}_{c_{1_j}}} \left[\bar{Q}_s\right]_{12} \left[B\right]^{-1} \frac{\partial[\bar{K}_s]}{\partial p_{s_i}} \left[B\right]^{-1} \left\{\bar{Q}_c\right\}_{2_j} \tag{16}$$

It should be noted that the calculation of all the control effectiveness parameters in Eq. (14) and all their derivatives in Eq. (16), for a given set of design variables, involves only one matrix inversion of order n_s where n_s is the number of elastic modes after truncation (16 in our case).

The variation of η_4 and $\partial\eta_4/\partial p_{s_2}$, divided by their base-line values, with the number of low frequency modes taken into account are shown in Fig. 5. The base-line values, calculated by all the data-base modes are η_4=0.216 and $\partial\eta_4/\partial p_{s_2}$=0.0079. The stars indicate the modes which will be actually truncated in the optimization. The convergence rates demonstrate the adequacy of the modal approach in considering control effectiveness in structural optimization. It should be noticed, however, that the convergence of the sensitivity derivatives is slower than that of η itself.

Sensitivity Derivatives and Constraints

The sensitivity derivatives of flutter dynamic pressure and gain and phase margins with respect to structural and control design variables are presented in Ref. 4. They are based on the neutral stability eigenvalue, the associated column and row eigenvectors and derivatives of $[\bar{A}]$ of Eq. (7), namely the system matrix before residualization. When the model is residualized, the full-size

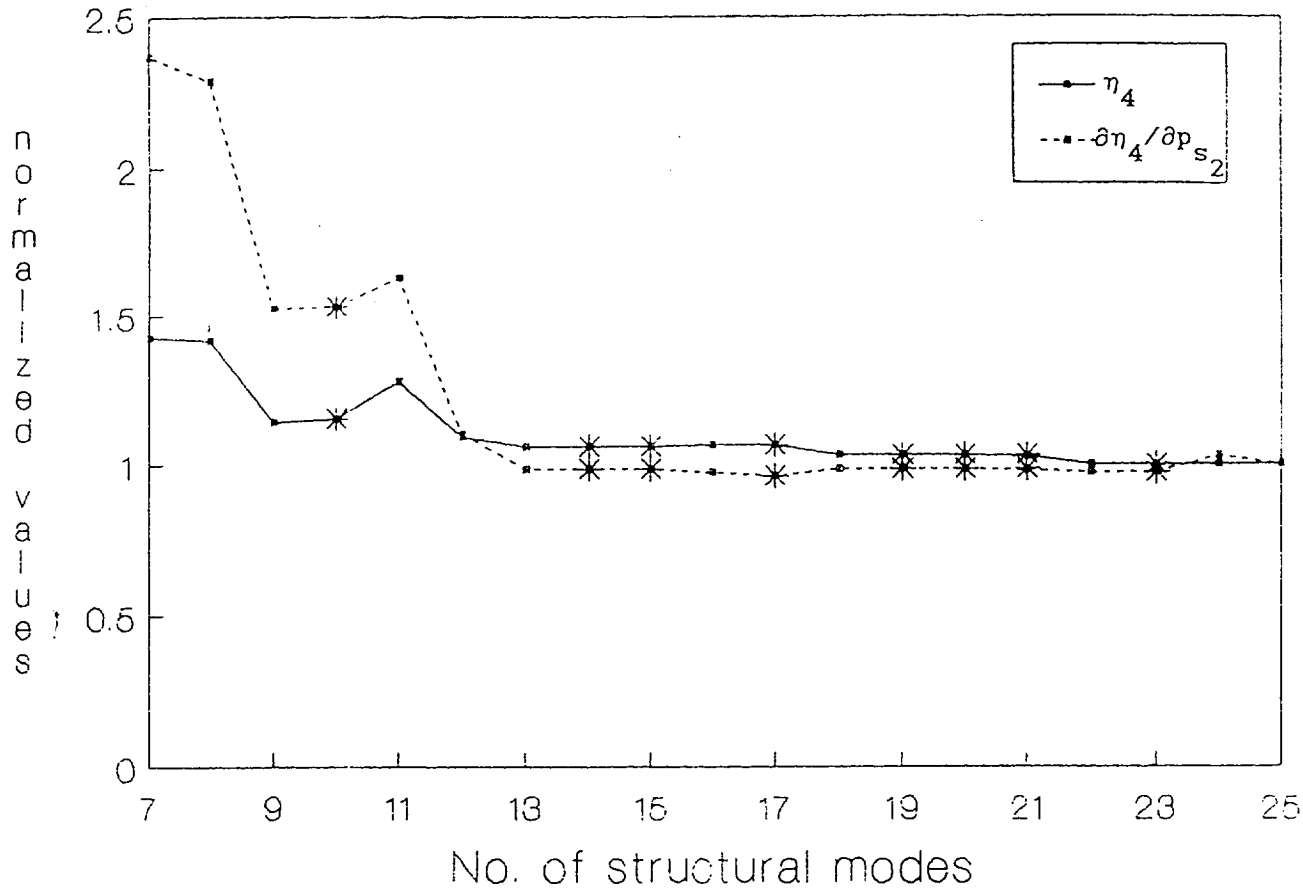

Fig. 5. Control effectiveness variations with number of structural modes taken into account.

column eigenvector is calculated from the reduced-order one as discussed after Eq. (12). The full-size row eigenvectors are calculated in a similar way but with Eqs. (11) and (12) transposed.

Equality constraints are defined as a linear dependency between the design variables of the form

$$\Sigma C_i p_i = C_o \tag{17}$$

One of the design variables, p_k which has a non zero C_k, is defined as a dependent variable. The differentiation of Eq. (17) with respect to an independent design variable, p_j, yields the constrained derivatives

$$\frac{\partial}{\partial \tilde{p}_j} = \frac{\partial}{\partial p_j} - \frac{1}{C_k}\left(C_j + \Sigma_i \frac{\partial C_i}{\partial p_j} p_i\right) \frac{\partial}{\partial p_k} \tag{18}$$

In our test-case, the rolling moment requirement of Eq. (1) is utilized by defining G_4 as a dependent gain, which yields the constrained sensitivity

derivatives with respect to other gains

$$\frac{\partial}{\partial \tilde{G}_j} = \frac{\partial}{\partial G_j} - \frac{\eta_j \bar{L}_{\delta_j}}{\eta_4 \bar{L}_{\delta_4}} \frac{\partial}{\partial G_4} \tag{19}$$

and the constrained sensitivity derivatives with respect to the structural design variables

$$\frac{\partial}{\partial \tilde{p}_{s_j}} = \frac{\partial}{\partial p_{s_j}} - \frac{1}{\eta_4 \bar{L}_{\delta_4}} \left(\sum_i \frac{\partial \eta_i}{\partial p_{s_j}} \bar{L}_{\delta_i} G_i \right) \frac{\partial}{\partial G_4} \tag{20}$$

The Optimization Process

Three cases of the base-line structure with different control gains are given in Table 3. All the cases satisfy the rolling requirement of Eq. (1) with $G_1=0.0$. Case 1 is with $G_2=G_4$ and $G_3=0$, which yields $q_f<q_d$. Since $\partial q_f/\partial G_4$ is relatively large and η_4 is relatively low, G_4 can be used to suppress flutter while the other gains compensate for the loss of rolling moment. This is utilized in cases 2 and 3 in which $q_f>q_d$ but the flutter and gain margin requirements of Eqs. (2) and (3) are not met. Even though the main participants in the flutter mechanisms of cases 2 and 3 are the same modes (3 and 4 of Table 1), the flutter frequency, gain margins and the derivatives are substantially different, which indicates a high sensitivity of the stability characteristics to parametric changes.

To obtain a balanced structural design, all the design variables associated with the -45° ply direction are constrained to be equal to the $+45^\circ$ ones. To avoid violation of stress requirements and to obtain a smooth design, all the structural variables are limited to $0 \le p_{s_i} \le \bar{p}_s$ where $\bar{p}_s=1.0$ in zones 1 and 2 of Fig. 3, 2.0 in zones 3 to 5, 3.0 in zones 6 to 8 and 4.0 in zones 9 to 11. The control gains are constrained to $G_1=0$ and the other $|G_i| \le \bar{G}$ where $\bar{G}$ is equal to either 0.09 or 0.1. The remaining independent design variables are the twenty two 0° and 45° structural variables and two control gains (G_2 and G_3).

A preliminary analysis indicated that the critical stability parameters are q_f and the positive GM_j values for j=2 to 4. Consequently, the cost function to be minimized is

$$J = e^{A_W(\Delta W-\Delta W_o)} + e^{A_f(q_{fo}-q_f)} + \sum_{j=2}^{4} e^{(GM_o-GM_j)} \tag{21}$$

where q_{f_o} and GM_o are the requested flutter dynamic pressure and gain margins,

parameter	Case 1	Case 2	Case 3
G_2	-0.0871	-0.0900	-0.1
G_3	0.0	-0.0900	-0.1
G_4	-0.0871	0.0203	0.0667
q_f(psi)	0.633	1.564	1.745
ω_f(rad/sec)	78.910	74.646	55.180
GM_2(db)	-	0.798	7.993
GM_3(db)	-	0.613	8.743
GM_4(db)	-	9.231	4.148
$\partial q_f/\partial G_2$	1.94	6.97	-1.62
$\partial q_f/\partial G_3$	2.81	9.30	1.27
$\partial q_f/\partial G_4$	5.00	45.04	-10.02
$\partial q_f/\partial \tilde{G}_2$	-3.82	-153.4	34.06
$\partial q_f/\partial \tilde{G}_3$	-15.86	-39.3	12.09

Table 3: Three Base-Line Design Cases with Different Control Gains

ΔW is the added weight, ΔW_o is the allowed weight penalty and A_W and A_f are cost weighting parameters. The sensitivity derivatives of J are

$$\frac{\partial J}{\partial p_i} = A_W w_i e^{A_W(\Delta W-\Delta W_o)} - A_f \frac{\partial q_f}{\partial p_i} e^{A_f(q_{fo}-q_f)} - \sum_{j=2}^{4} \frac{\partial GM_j}{\partial p_i} e^{(GM_o-GM_j)} \qquad (22)$$

where p_i is either a structural variable p_{s_i} or a gain G_i and w_i is the weight penalty associated with p_{s_i}=1.

A steepest descent optimization algorithm has been used to perform the four optimization cases presented in Tables 4 and 5. Case I of Table 4 has been performed to find the optimal gains, limited by $\bar{G}$=0.1, without changing the structure. The results are close to those of case 3 of Table 3. but with better q_f and gain margins. However, q_f does not satisfy the required margins. The

parameter	Case I gain only	Case II	Case III G_3=0	Case IV
$\bar{G}$	0.1	0.1	0.1	0.9
ΔW(lb)	0.	0.070	0.277	0.287
q_f(psi)	2.031	2.191	2.183	2.620
ω_f(rad/sec)	51.397	59.307	83.610	66.420
GM_2(db)	6.57	6.56	9.57	6.39
GM_3(db)	7.48	6.69	-	5.24
GM_4(db)	7.07	8.37	8.92	8.84
G_2	-0.0974	-0.0974	-0.1	-0.09
G_3	-0.0914	-0.0901	0.0	-0.09
G_4	0.0481	0.0435	-0.0315	0.0230

Table 4: Four optimization cases.

i	zone	ply direction (°)	Case II	Case III	Case IV
1	1	0	0.199	1.	0.
2	1	45	0.020	1.	0.
3	2	0	0.317	1.	0.
4	2	45	0.015	1.	0.
5	3	0	0.002	0.	0.
6	3	45	0.098	2.	0.
7	4	0	0.	0.	0.
8	4	45	0.157	2.	0.
9	5	0	0.014	0.	0.
10	5	45	0.035	2.	0.
11	6	0	0.	0.	0.
12	6	45	0.075	0.	0.
13	7	0	0.	0.	0.
14	7	45	0.	0.	0.
15	8	0	0.	0.	0.
16	8	45	0.	0.	0.
17	9	0	0.538	0.	4.
18	9	45	0.	0.	0.
19	10	0	1.346	0.092	4.
20	10	45	0.	0.	0.
21	11	0	0.	0.	4.
22	11	45	0.	0.	0.

Table 5: Structural changes (p_{s_i}) in Cases II to IV

simultaneous structure and gain optimization of Case II yields sufficient margins at the penalty of adding 0.07 lb to the structure. It can be noticed from Case II of Table 5 that the 0° plies in the wing root zones 9 and 10 and in

the wing tip zones 1 and 2 are the most effective. The 45° plies of zones 3 and 4 have also some effect while the others are either not effective or constrained to the minimum gage. Case III is the same as II but with G_3=0. The required margins are also met but with an additional weight penalty of 0.207 lb. The flutter frequency and the structural changes are substantially different than those of Case II. The 0° and 45° plies of zones 1 and 2, and the 45° plies of zones 3 to 5 achieve their maximum limits while all the others remain at or close to their minimum limits. Case IV is the same as Case II but with gain limits of $\bar{G}$=0.9. The optimization process stopped in this case when all the independent design variables reached their limits. The differences between the resulting structures of Table 5 demonstrate the importance of simultaneous structural and control optimization of aeroservoelastic systems.

The variations of q_f, ΔW, p_{s_6} and $p_{s_{21}}$ along the 10 step optimization process of Case III are plotted in Fig. 6. This case has been performed with a

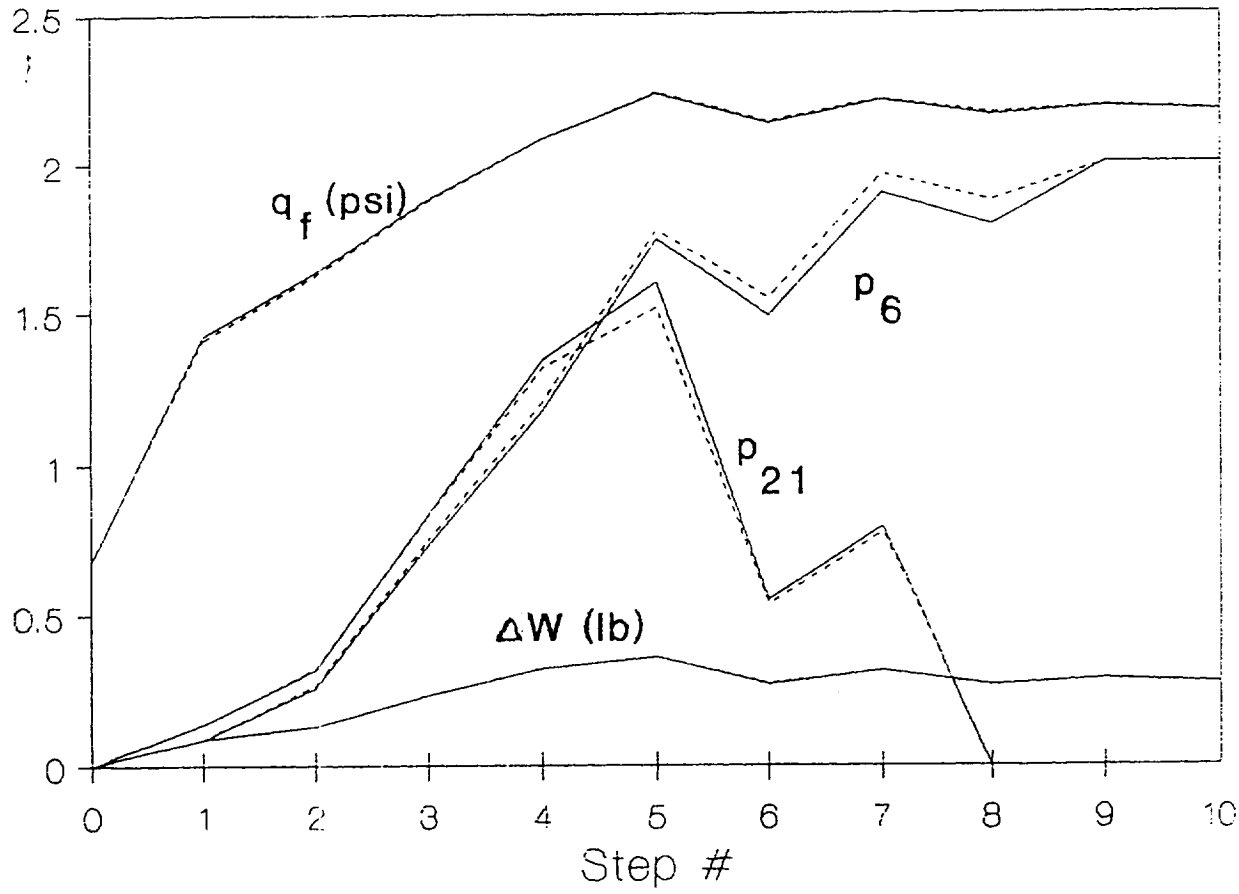

Fig. 6. Variations of flutter dynamic pressure, added weight and two structural variables along the optimization path, Case II.

34 state aeroservoelastic model (22 structural, 6 aerodynamic and 6 control states). The computation cpu time was about 5 min on a MicroVax 3200. The dashed lines of Fig. 6 are for the same optimization process but with all the 25 data-base modes yielding a 62 state aeroservoelastic model, which took about 32 cpu min. Figure 6 demonstrates the efficiency of the optimization process and

the accuracy of the reduced-size model relative to the full-size one.

Two NASTRAN model updates were performed with the p_s values of Cases III and IV of Table 5. The entire aeroservoelastic modeling process of Fig. 1 was repeated for each case, followed by root-locus stability analysis. All the new stability characteristics were within 3% of the associated ones in Table 4, which demonstrates the accuracy of the presented approach.

Conclusions

A systematic method for data-base construction, modeling and structural and/or control optimization of aeroservoelastic systems has been presented. The method is applicable to any objective function that can be analyzed by the normal modes approach and analytically differentiated with respect to the design variables. Standard, commercially available finite-element and unsteady aerodynamic computer codes can be used to construct the aeroelastic data-base. Application of Minimum-State rational approximations of the aerodynamic matrices yields a low number of aerodynamic states relative to the number of structural states. The weighting algorithm used to select modes for model size-reduction, and the dynamic residualization method have been shown to yield high-accuracy, reduced-order models. Sensitivity derivatives of flutter dynamic pressure and control margins have been extended to deal with residualized systems. Expressions for an efficient calculation of aeroelastic effectiveness parameters and their sensitivity derivatives have been presented and used to implement aircraft performance requirements. The ensemble of all these analytical and computational techniques yields an efficient, high-accuracy optimization process which can be used as a practical design tool of realistic modern aeronautical composite structures and control systems.

References

1. Livne, E., Shmit, L.A. and Friedmann, P.P., "Towards Integrated Multidisciplinary Synthesis of Actively Controlled Fiber Composite Wings", to appear in the J. of Aircraft, special issue on multidisciplinary optimization.

2. Giles, G.L., "Equivalent Plate Analysis of Aircraft Wing Box Structures with General Planform Geometry", J. of Aircraft, Vol. 23, No. 11, 1986, pp. 859-864.

3. Karpel, M., "Reduced-Order Aeroelastic Models via Dynamic Residualization", J. of Aircraft, Vol. 27, No. 5, 1990, pp. 449-455.

4. Karpel, M., "Sensitivity Derivatives of Flutter Characteristics and Stability Margins for Aeroservoelastic Design", J. of Aircraft, Vol. 27, No. 4, 1990, pp. 368-375.

5. Tiffany, S.H. and Adams, W.M. Jr., "Nonlinear Programing Extensions to Rational Approximation Methods of Unsteady Aerodynamic Forces", NASA TP-2776, July 1988.

6. Karpel, M., "Design for Active and Passive Flutter Suppression and Gust Alleviation", NASA CR-3482, Nov. 1981.

7. Karpel, M., "Time-Domain Aeroservoelastic Modeling Using Weighted Unsteady Aerodynamic Forces", J. of Guidance, Control and Dynamics, Vol. 13, No. 1, 1990, pp. 30-37.

8. Karpel, M. and Hoadley, S.T., "Physically Weighted Minimum-State Unsteady Aerodynamic Approximations", NASA TP (to be published).

9. Tiffany, S.H. and Karpel, M., "Aeroservoelastic Modeling and Applications Using Minimum-State Approximations of the Unsteady Aerodynamics", presented at the 30th SDM Conference, Mobile, Alabama, April 1989.

10. Karpel, M., "Extensions to the Minimum-State Aeroelastic Modeling Method", to appear in the AIAA Journal.

11. Karpel, M. and Sheena, Z., "Structural Optimization for Aeroelastic Control Effectiveness", Journal of Aircraft, Vol. 26, No. 5, 1989, pp. 493-495.